An Investigation of the Reaction of CH_3S with CO

L. C. Koch,[†,‡] Paul Marshall,[‡,§] and A. R. Ravishankara*[,†,‡]

National Oceanic and Atmospheric Administration, 325 Broadway, Boulder, Colorado, 80305, Department of Chemistry and Biochemistry, University of Colorado, Boulder, Colorado 80309, Cooperative Institute for Research in Environmental Sciences, University of Colorado, Boulder, Colorado 80309, and Department of Chemistry, University of North Texas, P.O. Box 305070, Denton, Texas 76203

Received: February 22, 2004; In Final Form: March 30, 2004

The reaction of CH_3S with CO was studied by using laser-induced fluorescence (LIF) to detect CH_3S radicals that were produced through pulsed laser photolysis of CH_3SSCH_3. There was no increased loss of CH_3S in the presence of CO. We place an upper limit of 1.4×10^{-16} cm^3 molecule^{-1} s^{-1} on the rate coefficient, k_1, for the reaction $CH_3S + CO \rightarrow$ products (1), based on the precision in our measurements. This upper limit applies between 208 and 295 K. The addition of O_2 did not enhance the rate coefficient for reaction 1. The reaction between CH_3S and CO is therefore not expected to be a significant source of OCS or loss process for CH_3S in the atmosphere. We also conclude that the reaction of CH_3SOO with CO is not sufficiently rapid to be a significant loss process for CH_3S in the atmosphere. The rate coefficients for the removal of electronically excited CH_3S ($CH_3S(A)$) at 295 K by CO, N_2, and O_2 were found to be $(8.0 \pm 0.2) \times 10^{-11}$, $(7.0 \pm 1.6) \times 10^{-12}$, and $(4.8 \pm 0.8) \times 10^{-12}$ cm^3 molecule^{-1} s^{-1} ($\pm 2\sigma$ precision), respectively. Ab initio calculations indicate that formation of a weakly bound complex between ground-state CH_3S and CO is thermodynamically unfavorable, and that there are significant barriers to $CH_3S{\cdot}CO$ adduct formation and its subsequent dissociation to $CH_3 + OCS$, consistent with our experimental observations.

Introduction

Tropospheric carbonyl sulfide (OCS) is believed to be a source of stratospheric sulfate.[1] The sources of OCS in the troposphere are not fully characterized, but include CS_2 oxidation, ocean emission, and biomass burning.[2] On the basis of the results of chamber experiments, it has been suggested that OCS is produced in the gas-phase oxidation of dimethyl sulfide (DMS, CH_3SCH_3).[3] DMS is produced by oceanic phytoplankton and is the largest natural source of sulfur in the troposphere. It is a short-lived compound that is rapidly oxidized by OH and NO_3. The annual production of DMS is approximately 50 times that of OCS. Therefore, a reaction that is a minor channel in the oxidation of tropospheric DMS could be a major source of OCS. The mechanism for OCS formation in the gas-phase oxidation of DMS has not been established, but it has been proposed that it involves CH_3S and H_2CS intermediates,[3] species which have been observed in DMS oxidation. The conversion of DMS to OCS would create a pathway from a short-lived, tropospheric source of sulfur to a longer lived stratospheric source.

In this study we investigated the reaction of CH_3S with CO as a possible source of OCS.

$$CH_3S + CO \rightarrow \text{products} \tag{1}$$

The overall reaction to produce OCS and CH_3 is exothermic, with a $\Delta_rH°(298K)$ of -2.30 ± 0.67 kcal mol^{-1}. Thermodynamic data are from Sander et al.[4] We suspected CH_3S could add to CO because both of these compounds form other adducts. For example, the CH_3S radical forms a complex with O_2, CH_3SOO.[5] Furthermore OH, which is isoelectronic with CH_3S, adds to CO.[4] The reaction of CH_3S with CO may go through an intermediate complex:

$$CH_3S + CO \underset{k_{-2}}{\overset{k_2}{\rightleftharpoons}} CH_3S{\cdot}CO \rightarrow OCS + CH_3 \tag{2}$$

It is also possible that O_2 is involved in the production of OCS through the formation of CH_3SOO or $CH_3S{\cdot}CO$ complexes and the reactions

$$CH_3SOO + CO \rightarrow OCS + CH_3O_2 \tag{3}$$

$$CH_3S{\cdot}CO + O_2 \rightarrow OCS + CH_3O_2 \tag{4}$$

In this study the loss of ground-state CH_3S was monitored by using laser-induced fluorescence (LIF). This was done in the presence and absence of CO, N_2, and O_2. Additionally, the rate coefficients for removal of electronically excited CH_3S ($CH_3S(A)$) by O_2 and N_2 were measured. A Stern−Volmer analysis of the laser-induced fluorescence signal from CH_3S in the presence of CO was carried out to investigate the possibility of complex formation. This analysis was supported by the direct measurement of the rate coefficient for $CH_3S(A)$ removal by CO. Finally, the measured rate coefficient for reaction of CH_3S with CO was rationalized in terms of ab initio calculations.

Experimental Section

Two types of experiments were done. One focused on the rate coefficient for the reaction of CH_3S in the ground electronic

* Address correspondence to this author.
† National Oceanic and Atmospheric Administration and Department of Chemistry and Biochemistry, University of Colorado.
‡ Cooperative Institute for Research in Environmental Sciences, University of Colorado.
§ University of North Texas.

10.1021/jp049193t CCC: $27.50
Published on Web 05/21/2004

state, $CH_3S(X)$, with CO, and the other examined the rate coefficient for removal of $CH_3S(A)$ by CO, O_2, or N_2. In the first type, temporal profiles of $CH_3S(X)$ in the presence of differing amounts of CO were measured. The delay time between the photolysis laser pulse that created CH_3S and the probe laser pulse that detected it was varied between 50 and 6000 μs. The signal at each photolysis-probe delay time was the result of averaging 200 laser shots. The temporal profile for the loss of CH_3S in the presence of excess CO can be described by

$$[CH_3S]_t = [CH_3S]_o e^{-k't} \tag{I}$$

Here, k' is the first-order rate coefficient for CH_3S loss, $k' = k_1[CO] + k_a$, k_1 is the rate coefficient for the reaction of CH_3S with CO, and k_a is the first-order rate coefficient for loss of CH_3S in the absence of CO. First-order rate coefficients (k') determined from CH_3S temporal profiles were plotted against CO concentration to determine k_1. One assumption is that other CH_3S loss processes, represented here by k_a, were constant as CO concentrations varied. The removal of $CH_3S(X)$ by CO was studied between 208 and 295 K.

The second type of measurement was to determine the rate coefficient for removal of $CH_3S(A)$ through collisions with CO, N_2, and O_2. CH_3S radicals were generated through photolysis, and after a 10 μs delay CH_3S fluorescence profiles were recorded. This 10 μs time delay was sufficient to thermalize CH_3S. CO, N_2, and O_2 concentrations were varied. The photomultiplier tube (PMT) output was recorded on a 300 MHz storage oscilloscope. Temporal profiles of the fluorescence were collected for 2 μs, a few lifetimes of CH_3S in our system. The first-order rate coefficient for $CH_3S(A)$ removal was calculated from the slopes of plots of the logarithm of the fluorescence signal versus time. The first-order rate coefficients were plotted against the concentration of CO, N_2, or O_2 to determine the rate coefficient for $CH_3S(A)$ removal. The rate coefficient for the removal of $CH_3S(A)$ by CO was measured between 210 and 295 K. The rate coefficients for removal of $CH_3S(A)$ by N_2 and O_2 were measured only at 295 K.

The experimental apparatus was described in a previous paper,[6] and will be briefly discussed here. The pulsed photolysis beam used to create the CH_3S radicals and the pulsed probe beam used to detect them were crossed at right angles to each other in the center of a jacketed, temperature-regulated glass cell. A PMT detected fluorescence orthogonal to the two beams. The direction of gas flow was perpendicular to the photolysis beam and parallel to the probe beam. Both lasers were run at 10 Hz. The photolysis beam had a cross-sectional area of 1 cm^2. The linear flow velocity of the gas in the photolysis region was kept at 10 cm s^{-1}, or greater, to avoid repeated photolysis of the gas mixture. Cooled methanol was flowed through the jacketed cell to regulate temperature. The temperature difference between the center of the detection region and the cell wall was measured under the gas flow rate and pressure conditions used to determine k_1. It was less than 0.5 K.

Dimethyl disulfide (DMDS), CH_3SSCH_3, was photolyzed at 248 nm with a pulsed KrF excimer laser to produce CH_3S radicals. A typical initial concentration of CH_3S, $[CH_3S]_o$, generated through photolysis was $\sim 10^{11}$ molecules cm^{-3}. $[CH_3S]_o$ was calculated from the concentration of DMDS in the reaction cell, the measured photolysis fluence, the absorption cross section of DMDS at 248 nm, (1.24×10^{-18} cm^2),[7] and the quantum yield for CH_3S production from DMDS photolysis (1.65).[8] The concentration of DMDS in the reaction cell ranged from 8×10^{12} to 1.3×10^{14} molecules cm^{-3} and was obtained from measured gas flow rates and pressure, and the known fraction of DMDS in a prepared mixture of DMDS in He. The concentration of DMDS in the prepared mixture was determined manometrically. The initial CH_3S concentration was kept below $\sim 10^{12}$ molecules cm^{-3} to minimize the contribution of the CH_3S self-reaction to the measured temporal profile.

The probe beam was obtained from a pulsed excimer laser pumped dye laser ($\sim$3 mJ $pulse^{-1}$, 0.05 cm^2 beam area) and it excited CH_3S at 371.2 nm. This wavelength corresponds to the $A(^2A_1) \leftarrow X(^2E)$ transition of CH_3S, with one quantum in the carbon−sulfur stretch, ν_3.[9] In the kinetic studies, fluorescence from CH_3S was recorded for 30 ns, beginning 50 ns after the probe beam fired. Fluorescence at wavelengths longer than 400 nm was isolated by a cutoff filter and then detected by the PMT. Scattered light from the probe beam was measured and subtracted from the fluorescence signal.

DMDS in He, the carrier gas (He), and the reactant (CO) were mixed prior to entering the cell. The helium flow was adjusted to bring the total pressure to between 40 and 55 Torr. All experiments were carried out with He buffer gas. CO from Spectra Gases with a purity of 99.99% was used directly from a cylinder. The CO concentration was calculated from gas flow rates and pressure and was between 10^{15} and 10^{17} molecules cm^{-3}. These high concentrations of CO influenced CH_3S diffusion out of the photolyzed region. In some cases CO was replaced with N_2 to determine how the composition of the gas mixture affected CH_3S loss in the absence of CO, which was mostly due to diffusion.

The possibility that O_2 increased the rate coefficient for the reaction between CH_3S and CO was investigated by measuring CH_3S decays in the presence of $(0.8-5) \times 10^{16}$ molecules cm^{-3} of O_2 and $(0.14-1.1) \times 10^{16}$ molecules cm^{-3} of CO at a total pressure of 41 Torr.

Results and Discussion

The measured first-order rate coefficient for CH_3S loss did not appear to be correlated with the CO concentration. The bimolecular rate coefficient, k_1, determined from plots of k' vs [CO] was frequently negative. We will discuss the measurements of k_1 and the negative values found here. Next we will describe our observations in the presence of O_2, and the implications for complex formation. Then we will review the rate coefficients for the removal of $CH_3S(A)$ by CO, O_2, and N_2. Finally, through a Stern−Volmer analysis of $CH_3S(A)$ fluorescence signal in the presence of CO, we will show that complex formation between $CH_3S(X)$ and CO was insignificant.

Temporal profiles of CH_3S measured in the presence of different CO concentrations at 295 K are shown in Figure 1. These decays were fit to eq I using a nonlinear least-squares analysis with each signal weighted by $(1/\sigma)^2$, where σ is the standard deviation of 200 measurements of the fluorescence signal at a certain reaction time. First-order rate coefficients, k', were obtained from these fits and plotted against the concentration of CO. A linear least-squares analysis of the k' values at various concentrations of CO yielded the rate coefficient k_1. Here $k' = k_1[CO] + k_a$ (Figure 2). Each value of k_1 is calculated from approximately 10 measurements of first-order loss rate coefficients (k' values). The majority of values found for k_1 were negative and the 2σ error bars were close to the size of the rate coefficient (Table 1).

Temporal decays of CH_3S in the presence of CO were also measured at 244 and $\sim$208 K. In all cases CH_3S temporal profiles were exponential and the time constant for decay was independent of the CO concentration. As was the case at 295

TABLE 1: Measured Values for the Rate Coefficient for the Reaction of $CH_3S(X)$ with CO[a]

T (K)	[CO][b]	[O_2][b]	[CH_3S]$_0$[c]	pressure (Torr)	laser fluence[d]	range of k' (s^{-1})	k_1[e]
295	0−6.5	0	1.2−11	44.5−52.5	3.0−3.3	90−150	−2.4 ± 1.6
295	0−15.5	0	4.4−5.8	38.4−46.9	6.0−7.7	200−260	−1.7 ± 1.3
295	0−6.9	0	0.91−1.3	49.0−53.0	6.2−7.0	90−140	−0.84 ± 1.94
295	0−1.1	4.55	1.5	40.8−41.3	5.5−6.7	90−210	−23 ± 12
295	0−1.2	3.0	1.8−2.1	39.9−41.3	8.2−9.0	20−170	16.0 ± 6.4
295	0−6.5	8.0−8.6	1.2−1.3	40.4−42.9	4.9−5.3	210−330	−4.8 ± 2.6
244	0−18	0	1.2−1.6	40.6−48.4	6.6−8.1	130−190	−2.23 ± 0.78
209	0−3.5	0	0.34−0.42	44.4−45.8	3.3−4.7	80−130	0.16 ± 2.58
208	0−22	0	1.2−1.3	41.2−47.8	7.6−9.4	100−170	−1.27 ± 0.48

[a] The bath gas always contained He, while some experiments also had oxygen. The rate coefficient is found from the slope of a linear least-squares fit of k' plotted vs concentration of CO, weighted by $(1/\sigma)^2$, where σ is the standard deviation of the first-order rate coefficient, and $k' = k_1[CO] + k_a$. N_2 was not present in these experiments. [b] 10^{16} molecules cm^{-3}. [c] 10^{11} molecules cm^{-3}. [d] mJ $pulse^{-1}$ cm^{-2}. [e] 10^{-16} cm^3 $molecule^{-1}$ s^{-1} $\pm 2\sigma$ (precision).

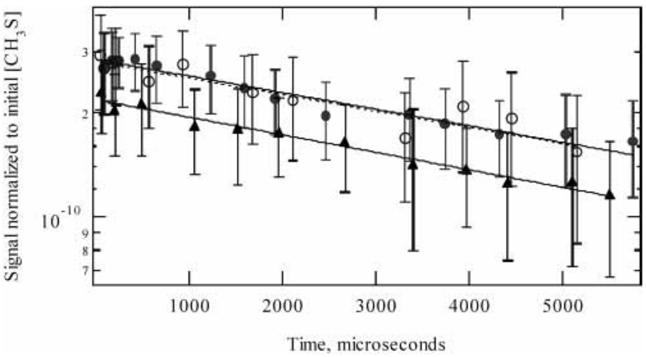

Figure 1. Representative temporal profiles of CH_3S in the presence of CO are shown. Traces were normalized to the initial CH_3S concentration. The lines are exponential fits weighted to $(1/\sigma)^2$. Error bars are 2σ. Concentrations (molecules cm^{-3}) were 1.2×10^{16} for CO and 9.8×10^{10} for [CH_3S]$_o$ (●), no CO and 9.1×10^{10} for [CH_3S]$_o$ (○), and 8.4×10^{16} for CO and 9.7×10^{10} for [CH_3S]$_o$, ▲. The shortest photolysis-probe delay was 50 μs. These decays were collected at 295 K.

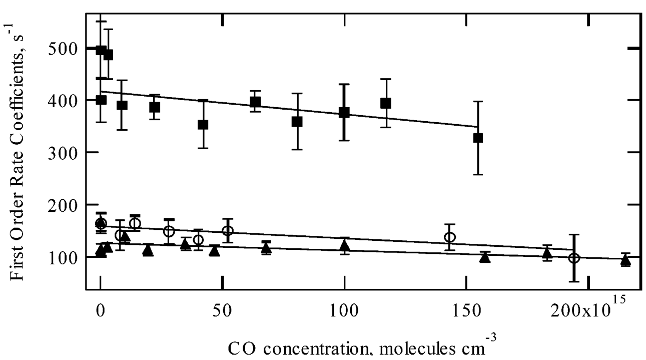

Figure 2. First-order rate coefficients for CH_3S loss in the presence of CO. Measurements were done at 295 (■ and ○) and 209 K (▲). Error bars shown are 2σ. Fitted lines were determined through linear least-squares analysis weighted to $(1/\sigma)^2$.

K, many of the determined values of k_1 were negative and had large error bars (Table 1). Due to these factors, we present upper limits for the values of k_1. Our upper limit for k_1 is 1.4×10^{-16} cm^3 $molecule^{-1}$ s^{-1}. This is the average 2σ uncertainty in the precision of the slope of the k' versus CO plot for multiple experiments performed in the presence of CO and He at 295 K. We recommend this upper limit at 244 K and ~208 K also, since experimental precision was similar.

The frequently negative values for k_1 require further examination. It is possible that CH_3S radicals were regenerated on the time scale of these observations, masking the loss of CH_3S due to reaction with CO. In addition, the observed negative k_1 values could be due to a reduction in the rate of CH_3S diffusion out of the reaction zone (the region where the photolysis and probe beams overlap), correlated with increases in CO concentration.

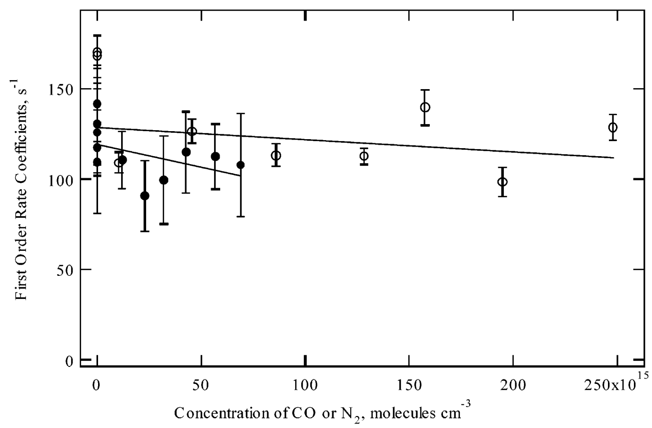

Figure 3. First-order rate coefficients for CH_3S loss in the presence of CO or N_2. These measurements were done at 295 K. Error bars shown are 2σ. The equation for the fitted line in the presence of CO (●) is $y = (119.5 \pm 8.0) - [(2.5 \pm 2.8) \times 10^{-16}][CO]$ and for N_2 (○) it is $y = (128.3 \pm 3.8) - [(6.5 \pm 3.0) \times 10^{-17}][N_2]$. The errors given for slope and intercept are 2σ, and are determined through linear least-squares fitting weighted to $(1/\sigma)^2$. The slope of each line represents the rate coefficient for the reaction. The negative values for the slopes are attributed to a reduction in the rate of diffusion of CH_3S out of the detection volume as CO or N_2 concentrations were increased. See text.

It is not obvious what process could regenerate CH_3S in our system. None of the products of DMDS photodissociation react with DMDS to generate CH_3S.[8] In addition, CO does not absorb at 248 nm. Therefore, we do not create excited CO that could react with DMDS to produce CH_3S, which is consistent with the exponential temporal profiles of CH_3S in the presence of CO. We conclude that secondary chemistry regenerating CH_3S was not the source of the measured negative rate coefficients.

Negative k_1 values may be due to reduced diffusion of CH_3S out of the detection region as the mole fraction of CO in the reaction mixture increased. CO concentrations were varied over a large range, from 10^{15} to 10^{17} molecules cm^{-3}, out of a total number density of about 1.3×10^{18} molecules cm^{-3}. The remainder of the flow was largely He. Changes in the rate of diffusive loss with gas composition have been noted previously.[10]

Temporal profiles of CH_3S were measured with N_2 in place of CO to investigate the effects of diffusion. N_2 has the same molecular weight as CO but is not expected to react with CH_3S. The measured rate coefficient for the loss of $CH_3S(X)$ in the presence of N_2 at room temperature is not distinguishable from that in CO. See Figure 3 and Table 2. As with CO, the slope of a plot of k' versus N_2 concentration was negative. It had a value

TABLE 2: Measured Rate Coefficient for the Loss of $CH_3S(X)$ in the Presence of N_2, k_{loss}

T (K)	$[N_2]^b$	$[CH_3S]_0^c$	pressure (Torr)	laser fluence^d	k_{loss}^e
295	0−25	1.4−1.7	41.2−48.8	4.3−5.7	0.045 ± 0.29
295	0−9.3	0.84−1.2	40.6−42.6	3.9−5.2	−6.9 ± 5.0

[a] These experiments were done to determine the effect of changing the nature of the bath gas on the rate of CH_3S diffusion. CO was not present. [b] 10^{16} molecules cm^{-3}. [c] 10^{11} molecules cm^{-3}. [d] mJ pulse^{-1}. [e] 10^{-16} cm^3 molecule^{-1} s^{-1} ± 2σ (precision).

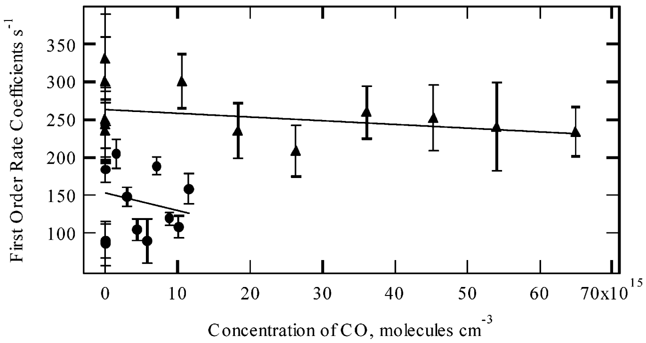

Figure 4. First-order rate coefficients for the loss of CH_3S in the presence of CO and O_2. The concentration of O_2 was held constant at 8.4×10^{15} (▲) and 4.6×10^{16} molecules cm^{-3} (●). CO concentrations were varied as shown. Error bars are 2σ. Lines are determined by linear least-squares fitting weighted to $(1/\sigma)^2$. The temperature was 295 K.

of -3.4×10^{-16} cm^3 molecule^{-1} s^{-1} as determined from theaverage of two measurements. This observation supports our hypothesis that the apparently negative rate coefficient measured for the reaction of $CH_3S(X)$ with CO can be attributed to a reduction in the rate of diffusion of CH_3S out of the detection region.

The role of O_2 in the reaction between $CH_3S(X)$ and CO was also investigated. The temporal profile of CH_3S in the presence of CO and O_2 may be controlled by reaction 3 and/or 4. We will discuss the reaction of CH_3SOO with CO (reaction 3), and then explore the reaction of CH_3SCO with O_2 (reaction 4).

If the CH_3SOO adduct formed and then reacted with CO, the rate coefficient for loss of CH_3S would increase upon addition of O_2. In the presence of O_2, the slope of k', the first-order rate coefficient for CH_3S loss, plotted versus CO was negative (Figure 4). This observation suggests that if CH_3SOO formed, the loss of this adduct due to reaction with CO was small or nonexistent. A value for k_3 can be estimated from the observed rate coefficient for CH_3S loss in the presence of CO and O_2 (Table 1), and the equilibrium coefficient for formation of CH_3SOO. The value of $\Delta_rG°$ was calculated from the reported $\Delta_rH°$ and $\Delta_rS°$.[5]

$$CH_3S + O_2 \Leftrightarrow CH_3SOO \qquad (5)$$

$$\Delta_rG°(298K) = -1.12 \pm 1.11 \text{ kcal mol}^{-1}$$

The equilibrium coefficient for reaction 5 at 298 K was calculated from $\Delta_rG°$(298K).

$$K_{eq}(298K) = \frac{[CH_3SOO]}{[CH_3S][O_2]} = (2.7 \pm 2.6) \times 10^{-19} \text{ cm}^3 \text{ molecule}^{-1} \quad (II)$$

The equilibrium coefficient here, calculated at 298 K, is expected to be comparable to the value at 295 K, the temperature at which our experiments were performed. If the adduct reacted with CO, the observed CH_3S loss rate in the presence of O_2 would then be

$$\frac{d[CH_3S]}{dt} = k_3[CH_3SOO][CO] = k_3K_{eq}[CH_3S][O_2][CO] \quad (III)$$

$$\frac{d[CH_3S]}{dt} = \{k_3K_{eq}[O_2]\}[CH_3S][CO] = k_{obs}[CH_3S][CO] \quad (IV)$$

Here, $k_{obs} = k_3K_{eq}[O_2]$. We measured k_{obs} to be less than 7.0×10^{-16} cm^3 molecule^{-1} s^{-1}. Using the above value for K_{eq} and the O_2 concentration of 5×10^{16} molecules cm^{-3} we determined an upper limit for k_3 of 5.2×10^{-14}cm^3 molecule^{-1} s^{-1}. The error bars on $\Delta_rG°$ and K_{eq} were deduced from the 2σ error bars reported for $\Delta_rH°$ and $\Delta_rS°$.[5] If the magnitude of the error bar is considered, the lower limit for K_{eq} is 7.3×10^{-21} cm^3 molecule^{-1}, which leads to an upper limit on k_3 of 1.9×10^{-12} cm^3 molecule^{-1} s^{-1}.

Removal of CH_3S in the presence of CO and O_2 may also take place via reaction 4, instead of reaction 3. If a weakly bound $CH_3S{\cdot}CO$ adduct formed rapidly after the photolysis laser pulse but before we observed CH_3S, decays of CH_3S might appear exponential with a very long time constant for CH_3S loss. The observed CH_3S loss rate coefficient would be slow because CH_3S would be replenished by decomposition of the adduct. The fluorescence signal normalized to CH_3S concentration would be reduced with the addition of CO if some CH_3S is sequestered in an adduct. Such a signal reduction was not seen, which was one indication that there was no adduct formation between CH_3S and CO. (See Figure 1.) However, CO does lead to the removal of $CH_3S(A)$, which one might expect to lead to a reduction in the CH_3S fluorescence signal in the presence of CO. This was not visible because fluorescence was collected for only 30 ns, beginning 50 ns after the probe pulse. The time scale was too short to observe quenching effects.

We performed a series of measurements to check for production of the $CH_3S{\cdot}CO$ adduct. The rate coefficient for removal of $CH_3S(A)$ by CO was measured, and a Stern−Volmer analysis of $CH_3S(A)$ fluorescence in the presence of CO was carried out. The Stern−Volmer analysis was supported by the direct measurement of rate coefficients for removal of $CH_3S(A)$ in the presence of CO. Additionally the rate coefficients for removal of $CH_3S(A)$ by N_2 and O_2 were measured.

The decay of fluorescence from $CH_3S(A)$ in the presence of N_2, CO, and O_2 was measured directly on nanosecond time scales to determine $k_{R(N_2,CO,O_2)}$, the rate coefficients for removal of $CH_3S(A)$ through collisions with N_2, CO, and O_2 at 295 K.

$$CH_3S(A) + M \rightarrow CH_3S(X) + M \qquad (k_R) \qquad (6)$$

In the above equation, M represents the colliding species, N_2, CO, or O_2. $CH_3S(X)$ was pumped to the A state and the temporal profile of the fluorescence was measured. Fluorescence profiles for removal of $CH_3S(A)$ by CO are shown in Figure 5, and can be described by:

$$F_t = F_0\, e^{-(k_{R(M)}[M]+k_A)t} \qquad (V)$$

F is the fluorescence signal, and k_A is the first-order rate coefficient for removal of $CH_3S(A)$ in the absence of N_2, CO, or O_2. The quantity k_A is the sum of $k_f + k_{R(He)}[He] + k_{R(DMDS)}[DMDS]$, where k_f is the rate coefficient for spontaneous fluorescence of $CH_3S(A)$, and $k_{R(He)}$ and $k_{R(DMDS)}$ are respectively the rate coefficients for removal of $CH_3S(A)$ by

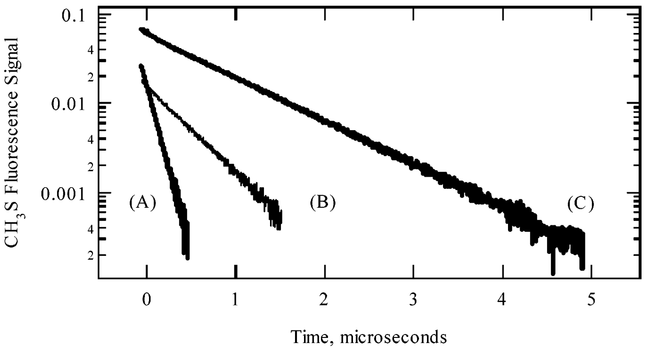

Figure 5. Typical CH_3S fluorescence decays in the presence of CO at 295 K. CO concentrations (molecules cm^{-3}) were 9.3×10^{16} (A), 1.5×10^{16} (B), and 0 (C). Decays were exponential over 2 to 3 lifetimes. Each decay is the average of 512 profiles.

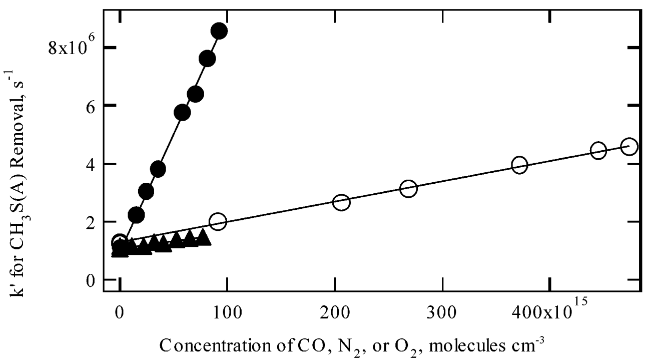

Figure 6. First-order rate coefficients for removal of $CH_3S(A)$ by CO (●), N_2 (○), and O_2 (▲) are plotted. The data shown were collected at 295 K. The linear fits are weighted to $(1/\sigma)^2$. The slope of each line is the rate coefficient for removal due to collisions with that species.

He and DMDS. Removal by He and DMDS were both included. While the rate coefficient for removal of $CH_3S(A)$ by He is small ($k \leq 1.6 \times 10^{-14}$ cm^3 $molecule^{-1}$ s^{-1}),[11] He was always present in our cell in large quantities (10^{18} molecules cm^{-3}). DMDS has a much larger rate coefficient for removal of $CH_3S(A)$ (7.1×10^{-10} cm^3 $molecule^{-1}$ s^{-1}),[12] but was present in lower concentrations (10^{13} molecules cm^{-3}). As a result their contributions to $CH_3S(A)$ removal were comparable.

The first-order rate coefficients for the removal of $CH_3S(A)$ at 295 K were obtained from the slope of a linear least-squares fit to the plot of $\ln(F)$ vs time. The first-order rate coefficients for removal by N_2, O_2, or CO were plotted against the concentration of N_2, O_2, or CO (Figure 6). The rate coefficient for removal, k_R, due to each species was determined from the slopes of these plots, which were calculated by using linear least-squares fits. The k_R measured for O_2 was $(4.78 \pm 0.76) \times 10^{-12}$ cm^3 $molecule^{-1}$ s^{-1} ($\pm 2\sigma$, precision in measurement of k_R), which is similar to the value of 5.4×10^{-12} cm^3 $molecule^{-1}$ s^{-1} ($\pm$10%), reported by Black[11] as the rate coefficient for removal of $CH_3S(A(^2A_1)\nu_3'=0)$ by O_2. The k_R for N_2 measured here was $(7.05 \pm 0.26) \times 10^{-12}$ cm^3 $molecule^{-1}$ s^{-1}, which is close to Black's measurement for the rate coefficient for removal of $CH_3S(A(^2A_1)\nu_3'=0)$ by N_2, 6.8×10^{-12} cm^3 $molecule^{-1}$ s^{-1} ($\pm$10%). The k_R for CO at 295 K was $(8.07 \pm 0.32) \times 10^{-11}$ cm^3 $molecule^{-1}$ s^{-1} ($\pm 2\sigma$, precision in measurement of k_R). There are no known measurements for comparison. Removal by CO was close to 10 times faster than by N_2 or O_2. The larger rate coefficient for removal by CO could be due to a reaction between $CH_3S(A)$ and CO or a resonant energy transfer to an electronic state of CO. Collisional energy transfer from $CH_3S(A)$ to CO is not expected to be stronger than with O_2 or N_2, as CO does not absorb near 370 nm, the excitation wavelength of $CH_3S(A)$. In addition, CO does not have a low-lying electronic or excited vibrational state at this energy. Therefore, we suspect there is a reaction between $CH_3S(A)$ and CO.

TABLE 3: Measured Values for the Rate Coefficient for Removal of $CH_3S(A)$ by CO, $k_{R(CO)}$, at Temperatures between 295 and 210 K

T (K)	k_R[a]
295	8.07 ± 0.32
271	8.24 ± 0.28
244	8.68 ± 0.50
242	9.19 ± 0.63
231	8.49 ± 0.24
210	9.09 ± 0.27

[a] 10^{-11} cm^3 $molecule^{-1}$ s^{-1} $\pm 2\sigma$ (precision).

The rate coefficient for removal of $CH_3S(A)$ by CO was also measured at lower temperatures (Table 3). There was a weak temperature dependence in the rate coefficient that resulted in higher values at lower temperatures (Figure 7). The temperature dependence can be described by $k_{R[CO]} = [(6.10 \pm 0.79) \times 10^{-11}]e^{(82\pm31)K/T}$ cm^3 $molecule^{-1}$ s^{-1}. Errors are 2σ, based on a linear least-squares fitting to the data, each data point weighted by $(1/\sigma)^2$.

A Stern−Volmer analysis was performed to determine if a complex involving CH_3S and CO formed. In this analysis, the CH_3S fluorescence collected in the presence of CO was integrated over time and considered to be proportional to the concentration of $CH_3S(A)$. In these experiments only fluorescence at wavelengths longer than 400 nm was detected but this is proportional to the total fluorescence and the $CH_3S(A)$ created, unless collisions with CO shift the fluorescence spectra. The collected fluorescence can be related to the concentration of the excited species by the expression:

$$\text{integrated fluorescence (IF)} = C\int_0^\infty [CH_3S\,(A)]\,dt = C\int_0^\infty [CH_3S(A)]_0 e^{(-k_A - k_{R(M)}[M])t}\,dt \quad \text{(VI)}$$

Here C is a proportionality constant, and the other terms retain their previous definitions. Integrating this expression gives:

$$IF = C[CH_3S(A)]_0\left[\frac{e^{(-k_A - k_{R(M)}[M])t}}{-k_A - k_{R(M)}[M]}\right]_0^\infty = \frac{C[CH_3S(A)]_0}{k_A + k_{R(M)}[M]} \quad \text{(VII)}$$

The expression is rearranged to describe a Stern−Volmer plot:

$$\frac{1}{IF} = \frac{k_A}{C[CH_3S(A)]_0} + \frac{k_{R(M)}[M]}{C[CH_3S(A)]_0} \quad \text{(VIII)}$$

The reciprocal of IF was plotted against the concentration of CO (Figure 8). The ratio of the slope to the intercept will be equal to k_R/k_A as long as other loss processes such as complex formation are not happening. Independently, k_R and k_A were determined from respectively the slope and intercept of the plot of the first-order rate coefficient for fluorescence decay vs concentration of CO, N_2, or O_2. The ratios of k_R/k_A in the presence of CO were then compared to the ratios of slope/intercept from the Stern−Volmer plots (Table 4). Even though there is a large uncertainty in the slope/intercept ratio, as expected in Stern−Volmer analysis, the agreement shown in Table 4 indicates that adduct formation was minimal or nonexistent.

The rate coefficient for removal of initially prepared $CH_3S(A)$ fluorescence in the presence of CO was measured at 295, 271,

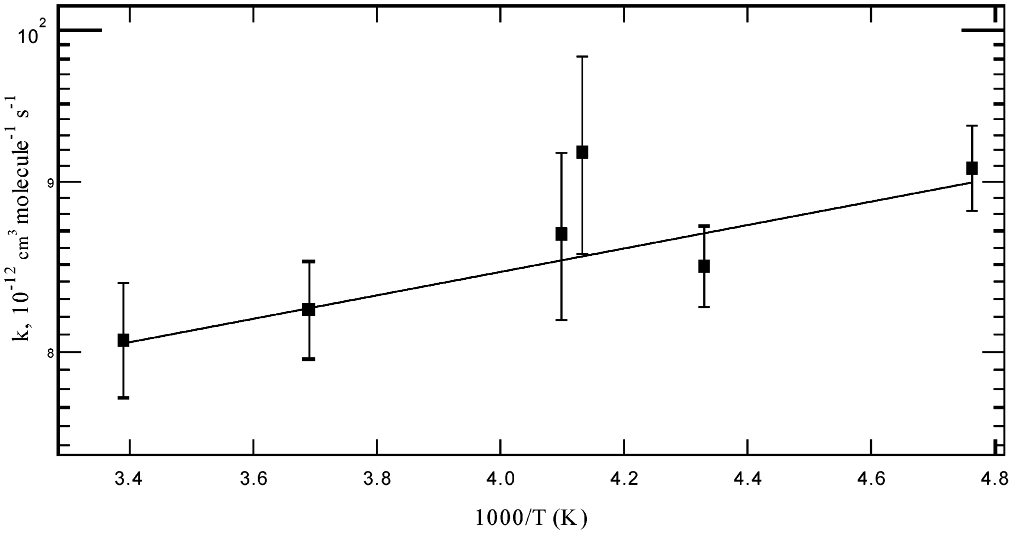

Figure 7. Arrhenius plot for the rate coefficient for removal of CH_3S(A) by CO. Error bars are 2σ. A linear least-squares fitting to the data, weighted to $(1/\sigma)^2$, is shown.

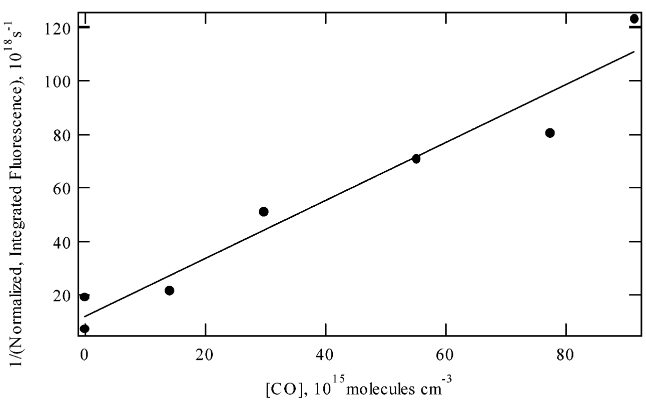

Figure 8. The data for CH_3S(A) signal depletion by CO plotted in a Stern−Volmer plot. These data were collected at 243 K. The ratio of slope/intercept is $(9.0 \pm 4.4) \times 10^{-17}$ cm^3 molecule^{-1}, which agrees well with $(8.5 \pm 1.1) \times 10^{-17}$ cm^3 molecule^{-1}, the ratio of measured values, k_R/k_A. See text.

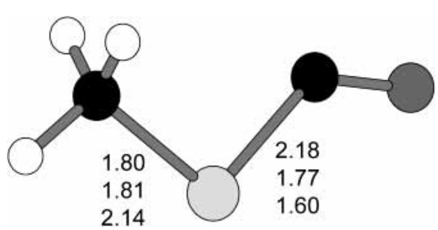

Figure 9. Geometries of two transition states and an intermediate for the reaction $CH_3S + CO \rightarrow CH_3 + OCS$, calculated at the MP2=full/6-31G(d) level of theory. The structure shown is that of the intermediate CH_3SCO adduct. The transition states are similar. The two carbon−sulfur bond lengths are given in Å, and the three numbers correspond to (top) TS1 for adduct formation from $CH_3S + CO$, (middle) adduct, and (bottom) TS2 for dissociation to $CH_3 + OCS$. Full coordinates are given in Table S3.

244, 242, 231, and 210 K. Stern−Volmer analyses were carried out at all these temperatures (Table 4). The ratio of the measured k_R and k_A agreed well with the ratio of slope/intercept from the Stern−Volmer plots. Even at the lowest temperature measured, where complex formation is thermodynamically most favored, there was no indication of complex formation between CO and ground-state CH_3S. We conclude that $CH_3S{\cdot}CO$ complex formation did not happen to a significant extent even at 210 K, the lowest temperature studied.

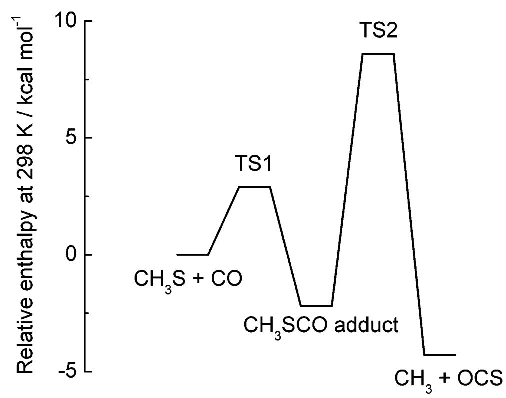

Figure 10. Relative enthalpies of reactants, transition states, intermediate, and products for the reaction $CH_3S + CO \rightarrow CH_3 + OCS$ at 295 K, computed via the Gaussian-3 method (see text).

TABLE 4: Ratios of Slope/Intercept from Stern−Volmer Plots, and Ratios of k_R/k_A Determined from the Direct Measurements of CH_3S Fluorescence Profiles[a]

T (K)	slope/intercept from Stern−Volmer plots[b]	measured k_R/k_A[b]
210	13 ± 9	9.9 ± 1
228	7 ± 2	8.5 ± 0.9
243	9 ± 4	8.5 ± 1.1
245	7 ± 2	10 ± 2
273	7 ± 5	8.0 ± 0.6
295	7 ± 6	7.5 ± 0.5

[a] The value of k_R was determined from the slope, and k_A was determined from the intercept of the plot of the first-order rate coefficient for CH_3S(A) fluorescence decay vs concentration of CO. [b] In units of 10^{-17} cm^3 molecule^{-1}.

Computational Analysis

The potential energy surface for the interaction of CH_3S(X) and CO was investigated at the Gaussian 3 level of theory.[13] Calculations were carried out with the GAUSSIAN98 program suite.[14] In brief, geometries of reactants, intermediates, transition states, and products were initially optimized at the HF/6-31G(d) level of theory to obtain vibrational frequencies. These frequencies were scaled by a standard factor of 0.8929 to account for anharmonicity and lack of electron correlation, and are listed in Table S1. They were employed for evaluation of zero-point energy corrections, of thermodynamic functions, and of partition functions. The thermodynamic and partition function terms included treatment of torsions as hindered internal rotors.[15] The geometries were refined via MP2=full/6-31G(d) theory (summarized in Table S2 and Figure 9) and used to estimate rotational partition functions for a series of single-point calculations which approximate complete QCISD(T)=full/G3Large energy calculations (see Table S3).[13]

The CH_3S radical has some special features. The equilibrium geometry has C_s symmetry (and is employed for the ab initio energy) but the energy difference between the three equivalent C_s isomers and the C_{3v} structure is less than the energy of one vibrational quantum for the mode corresponding to the distortion. This is an example of dynamic Jahn−Teller distortion.[16] For the purposes of calculating partition functions, a rotational symmetry number of 3 was assumed. There is also spin−orbit splitting of the ^2E ground state into $J = {}^1/_2$ and ${}^3/_2$ components separated by 259 cm^{-1},[17] and accordingly the nonrelativistic ab initio energy in Table S3 includes a downward correction of half this amount, 0.4 kcal mol^{-1}.

Figure 9 shows the geometry of a bound CH_3SCO species. Fitting the frequency for torsion about the central C−S bond of 98 cm^{-1} to a sinusoidal potential[18] yields a small rotational barrier of 0.5 kcal mol^{-1}. The ab initio data suggest that the adduct is bound by only 2.2 kcal mol^{-1} at 298 K. The equilibrium constant was evaluated via partition functions at 200 K to be about 10^{-27} cm^3 $molecule^{-1}$. Allowance of 2 kcal mol^{-1} error limits in the computed binding energy implies that, even with a high CO concentration of 10^{17} molecules cm^{-3}, only about 1 part in 10^8 or less of the CH_3S would be bound as a complex at equilibrium. This is in accord with the observed lack of adduct formation.

The adduct might act as a short-lived intermediate in the formation of CH_3 + OCS. We have characterized the reaction path via the adduct, and show the results in Figure 10. There are significant enthalpy barriers at 298 K to both addition of CH_3S to CO and then dissociation of CH_3SCO to CH_3 + OCS, of 2.9 and 8.6 kcal mol^{-1}, respectively, relative to CH_3S + CO. The latter value is probably an underestimate because OCS is known to be a difficult molecule for G3 analysis,[13] and the overall enthalpy change for reaction 1 to produce OCS and CH_3 is calculated to be −4.3 kcal mol^{-1}, which is 2.0 kcal mol^{-1} too negative relative to experiment.[4] Some of this error likely makes the calculated energy of the transition state leading to OCS too low as well. This large second barrier makes OCS formation negligibly slow, in accord with our observations here.

Transition state theory[19] yields the high-pressure limit for addition of CH_3S to CO, and at room temperature the predicted rate coefficient is $k \approx 3 \times 10^{-16}$ cm^3 $molecule^{-1}$ s^{-1}. Thus addition might in principle be measurable, especially at higher temperatures, except that, as noted above, this process is thermodynamically unfavorable and will result in rapid decomposition of the adduct back to reactants.

Atmospheric Implications

The CH_3S radical is an intermediate in the DMS oxidation mechanism that leads to longer lived sulfur species including SO_2. CH_3S is known to react rapidly with O_3 and NO_2. The reaction between CH_3S and CO will not be a significant loss process for CH_3S in the atmosphere due to the small rate coefficient measured here. In addition, the reaction of CH_3S with CO will not be a significant source of OCS. Annually, about 20 Tg of sulfur is emitted to the atmosphere as DMS, and the annual production of OCS is about 0.39 Tg of sulfur.[2] If one assumes all DMS is oxidized to CH_3S, the maximum contribution of this reaction to OCS production can be estimated. The contribution of a competing channel will be largest under low oxidant conditions. For low ozone and NO_2 concentrations, 10 ppbv and 3 pptv, respectively, and a high CO concentration of 100 ppbv, the reaction of CH_3S with CO would contribute 1% to the annual production of OCS, using the upper limit of 1.4×10^{-16} cm^3 $molecule^{-1}$ s^{-1} for k_1. Therefore, the reaction of CH_3S + CO is not a substantial global source of OCS.

It is possible that a complex between CH_3S and CO forms with the rate coefficient k_1, and decomposes with the rate coefficient k_{-1}. A rough estimate for an upper limit on K_{eq}, k_1/k_{-1}, can be determined from the uncertainties in the ratios of k_R/k_A (Table 4). Based on these, 10% of CH_3S could be bound in an adduct with CO, leading to an upper limit for K_{eq} of 10^{-18} cm^3 $molecule^{-1}$. This upper limit is conservative, and much larger than the value calculated above with ab initio theory. Under typical atmospheric conditions, with a CO concentration of 80 ppbv, 0.0002% of CH_3S would be bound up as $CH_3S{\cdot}CO$. Due to its low concentration, sequestration in this adduct will not reduce the rate of CH_3S removal by O_3 or NO_2. As well, our observations show that the reaction of CH_3SOO with CO is negligible.

Conclusions

Kinetic studies of the reaction of CH_3S with CO and measurements of the rate coefficient for removal of CH_3S(A) by CO between ∼210 and 295 K show that CH_3S does not significantly bind to CO, or react to form OCS (upper limit 1.4×10^{-16} cm^3 $molecule^{-1}$ s^{-1}) even in the presence of O_2. These results are consistent with a calculated ab initio potential energy surface, which indicates that adduct formation is not thermodynamically favorable and that there are large energy barriers to the addition of CH_3S to CO and to dissociation of a $CH_3S{\cdot}CO$ adduct to CH_3 + OCS. The reaction between CH_3S and CO is not a significant atmospheric source of OCS or loss process for CH_3S.

Acknowledgment. This work was supported by NOAA's Climate and Global Change Program. L. C. Koch appreciates support from CIRES through the Graduate Research Fellows Program. P. Marshall acknowledges support from the Robert A. Welch Foundation (Grant B-1174) and use of computer facilities at the National Center for Supercomputing Applications (Grant CHE000015N) and the Wright Laboratory, Wright-Patterson AFB.

Supporting Information Available: Ab initio data for reactants, transition states, intermediate, and products for the reaction CH_3S + CO → CH_3 + OCS; Table S1 summarizing rotational constants and frequencies, Table S2 showing the Cartesian coordinates, and Table S3 giving the Gaussian-3 energies, thermal corrections, and relative enthalpies. This material is available free of charge via the Internet at http://pubs.acs.org.

References and Notes

(1) Crutzen, P. J. *Geophys. Res. Lett.* **1976**, *3*, 73.
(2) Seinfeld, J. H.; Pandis, S. N. *Atmospheric Chemistry and Physics*; John Wiley & Sons: New York, 1998.
(3) Barnes, I.; Becker, K. H.; Patroescu, I. *Geophys. Res. Lett.* **1994**, *21*, 2389.
(4) Sander, S. P.; Friedl, R. R.; Golden, D. M.; Kurylo, M. J.; Huie, R. E.; Orkin, V. L.; Moortgat, G. K.; Ravishankara, A. R.; Kolb, C. E.; Molina, M. J.; Finlayson-Pitts, B. J. *Chemical Kinetics and Photochemical Data for Use in Atmospheric Studies*; Jet Propulsion Laboratory Publication No. 02-25, 2003, http://jpldataeval.jpl.nasa.gov/
(5) Turnipseed, A. A.; Barone, S. B.; Ravishankara, A. R. *J. Phys. Chem.* **1992**, *96*, 7502.

(6) Turnipseed, A. A.; Barone, S. B.; Ravishankara, A. R. *J. Phys. Chem.* **1993**, *97*, 5926.

(7) Hearn, C. H.; Turcu, E.; Joens, J. A. *Atmos. Environ.* **1990**, *24A*, 1939.

(8) Barone, S. B.; Turnipseed, A. A.; Gierczak, T.; Ravishankara, A. R. *J. Phys. Chem.* **1994**, *98*, 11969.

(9) Chiang, S. Y.; Lee, Y. P. *J. Chem. Phys.* **1991**, *95*, 66.

(10) Herndon, S. C.; Froyd, K. D.; Lovejoy, E. R.; Ravishankara, A. R. *J. Phys. Chem.* **1999**, *103*, 6778.

(11) Black, G.; Jusinski, L. E. *J. Chem. Soc.*, *Faraday Trans.* **1986**, *2*, 2143.

(12) Black, G.; Jusinski, L. E. *J. Chem. Phys.* **1986**, *85*, 5379.

(13) Curtiss, L. A.; Raghavachari, K.; Redfern, P. C.; Rassolov, V.; Pople, J. A. *J. Chem. Phys.* **1998**, *109*, 7764.

(14) Frisch, M. J.; Trucks, G. W.; Schlegel, H. B.; Scuseria, G. E.; Robb, M. A.; Cheeseman, J. R.; Zakrzewski, V. G.; Montgomery, J. A., Jr.; Stratmann, R. E.; Burant, J. C.; Dapprich, S.; Millam, J. M.; Daniels, A. D.; Kudin, K. N.; Strain, M. C.; Farkas, O.; Tomasi, J.; Barone, V.; Cossi, M.; Cammi, R.; Mennucci, B.; Pomelli, C.; Adamo, C.; Clifford, S.; Ochterski, J.; Petersson, G. A.; Ayala, P. Y.; Cui, Q.; Morokuma, K.; Malick, D. K.; Rabuck, A. D.; Raghavachari, K.; Foresman, J. B.; Cioslowski, J.; Ortiz, J. V.; Baboul, A. G.; Stefanov, B. B.; Liu, G.; Liashenko, A.; Piskorz, P.; Komaromi, I.; Gomperts, R.; Martin, R. L.; Fox, D. J.; Keith, T.; Al-Laham, M. A.; Peng, C. Y.; Nanayakkara, A.; Challacombe, M.; Gill, P. M. W.; Johnson, B.; Chen, W.; Wong, M. W.; Andres, J. L.; Gonzalez, C.; Head-Gordon, M.; Replogle, E. S.; Pople, J. A. *Gaussian 98*, Revision A.9; Gaussian, Inc.: Pittsburgh, PA, 1998.

(15) Lewis, G. N.; Randall, M.; Pitzer, K. S.; Brewer, L. *Thermodynamics*, 2nd ed.; McGraw-Hill: New York, 1961; Chapter 27.

(16) Bent, G. D. *J. Chem. Phys.* **1990**, *92*, 1547.

(17) Chiang, S. Y.; Lee, Y. P. *J. Chem. Phys.* **1991**, *95*, 66.

(18) Benson, S. W. *Thermochemical Kinetics*, 2nd ed.; Wiley: New York, 1976; Chapter 3.

(19) Steinfeld, J. I.; Francisco, J. S.; Hase, W. L. *Chemical Kinetics and Dynamics*; Prentice Hall: Englewood Cliffs, NJ, 1989; Chapter 10.